RSC Advances

ROYAL SOCIETY OF CHEMISTRY

www.rsc.org/advances

Cite this: DOI: 10.1039/c0xx00000x

www.rsc.org/xxxxxx

ARTICLE TYPE

Enhanced electron field emission properties from hybrid nanostructures of graphene/Si tip array

Tinghsun Chang[a], Fangwei Lu[a], Srinivasu Kunuku[b], Kehchyang Leou[b], Nyanhwa Tai*[a] and Inan Lin*[c]

Received (in XXX, XXX) Xth XXXXXXXXX 20XX, Accepted Xth XXXXXXXXX 20XX
DOI: 10.1039/b000000x

High efficiency with excellently stable electron field emitters based on monolayer graphene coated on well-aligned Si tip (graphene/SiT) arrays fabricated, by a simple transfer method is demonstrated. The graphene monolayer is coated on the Si tip array using a chemical vapor deposition process, while the SiTs are prepared through the etching process of a Si substrate. The novel heterostructure field emitter enhanced electron tunneling, as a result, exhibits better emission property. In addition, the fabricated microplasma devices based on the graphene/SiT heterostructure are closely correlated to the field emission properties of the graphene/SiT materials. The monolayer graphene supported on vertical SiTs provides for the protruded nanostructure, which locally enhances the electric field and thus improves the field emission and the plasma illumination characteristics.

1. Introduction

The electron field emission (EFE) properties of nanostructured materials, such as carbon nanotubes (CNTs)[1-4], graphene[5-7], graphene oxide (GO)[8,9], carbon nanosheets[10-12], Si nanowires, and nanostructured diamond films have caught great attention from researchers. Among these nanostructures, graphene and GO have particularly attracted enormous attention. Graphene with two-dimensional graphitic nanostructure and a one-carbon-atom-thick honeycomb crystal lattice has high aspect ratio (the ratio of lateral size to thickness), excellent chemical stability, unique electrical properties and high transparency, apart from possessing an intrinsic flexible structure and good mechanical properties. These properties make graphene a promising material for the application of field emitters[13-15]. Recently, the EFE properties of graphene and few-layer graphene films prepared by different techniques have been reported[6,7,16-18].

One-dimensional nanostructures such as nanotubes, nanowires, nanorods, and nanocones attract great interest in the applications of electronic and photonic nanodevices owing to their high aspect ratio and low dimensional effect, which are essential elements for good EFE performance[19-23]. Nanoscale heterostructures consisting of different components are important building blocks for functional devices to achieve multifunctionality, such as high emission efficiency and superior electron mobility[24,25]. Silicon-based nanoemitters such as silicon nanowires or nanoarrays are superior to other nanowire templates because of their compatibility with Si materials and greater potential for integration with Si devices to form active electron field emitters[26,27]. Incorporation of graphene and sharpened Si tips (SiTs), which contributes to the highly efficient performance of a target application device, leads to the exceptional properties of nanoscale heterostructure silicon-based nanodevices.

Drops of solution containing the required material have been used to deposit graphene sheets onto the one-dimensional nanostructures for field emission applications, e.g. graphene or GO coated on the top of nanowires or nanotips. However this approach is difficult to achieve large-scale uniform deposition[9,28,29]. In this work, we demonstrate the fabrication of heterostructure field emitters using a simple and robust technique for depositing graphene on SiT (graphene/SiT) arrays, which can be practical electron sources for advanced devices. We observe that the EFE and the plasma illumination (PI) characteristics of the fabricated devices markedly enhance when the graphene/SiT array field emitters are used as the cathodes.

2. Experimental

2.1 Preparation of graphene/SiT arrays

A schematic description of the fabrication process of graphene/SiT array field emitters is illustrated in Figure 1. A photoresist (PR, EPG512) film of thickness 1.0 μm is spin-coated on a Si substrate. This is then patterned by a conventional photolithographic process to form a square periodic pattern of size 6 μm x 6 μm with 10 μm separations (step 1, Figure 1). Prior to the spin-coating, the Si substrate is

pre-cleaned by rinsing in water-diluted hydrogen peroxide/ammonium hydroxide and hydrogen peroxide/sulfuric acid solutions[30]. The patterned Si substrate is then coated upon using a thin Ag film (~40 nm) with a dc sputter deposition system (Helix) at a power of 50 W in argon partial pressure of 5 mtorr (step 2, Figure 1). The SiT arrays are then obtained by a self-galvanic process which occurs when immersing the Ag-coated patterned Si substrate in an etching solution [HF (4.60 M)+H_2O_2 (0.44 M)] at room temperature for 7 min (step 3, Figure 1)[31]. This is followed by the removal of the Ag and PR coatings using nitric acid, acetone and deionized water, after which the film is dried (step 4, Figure 1). The fabricated SiT arrays are then dipped in a 30 wt.% KOH solution for 30 min to sharpen the SiTs (step 5, Figure 1). The graphene used in our work is grown on Cu foils by the chemical vapor deposition method[32]. For graphene transfer, a layer of polymethyl methacrylate (PMMA, 950,000 MW, 6 wt.%) mixed with anisole is spin-coated on the as-grown graphene/Cu foil at a speed of 1500 rpm for 30 s and heated on a hot plate at 130^{o}C for 10 min. The Cu foil is etched in a solution containing H_2O_2 (30% w/v) and (0.1 M) HCl for 2 h and the PMMA on graphene (PMMA/graphene) film is floated on the surface of the solution. The PMMA/graphene film is then rinsed four times using deionized water to remove the residual etchant. This is then placed on the target substrate which contains the SiT arrays on it, followed by a drying process at room temperature (step 6, Figure 1). Finally, acetone is used to remove PMMA and the sample with graphene uniformly adherring onto the SiT arrays is obtained (step 7, Figure 1).

2.2 Structure characterizations and measurements of electric properties

The morphologies of the films are examined using field emission scanning electron microscope (FESEM; JEOL-6500). The bonding structure of the films is characterized at room temperature using Raman spectroscopy (Lab Raman HR800, Jobin Yvon) which is equipped with a 514 nm laser as the excitation source. The thickness and roughness of graphene are measured by atomic force microscopy (AFM, Veeco Nanoscope 3100). High resolution transmission electron microscopic images (HRTEM; JEOL-2100F) are examined to characterize the grahenen coated on Si tips.

The EFE properties of the bare SiTs, graphene/Cu foil, and graphene/SiTs are measured using a parallel plate apparatus, in which the sample-to-anode distance is controlled using a micrometer spacer. The current density-electric field (J_e-E) characteristic curves are measured using an electrometer (Keithley 2410) at a pressure of 10^{-6} torr. To characterize the PI properties of the parallel plate type devices, an indium tin oxide (ITO) coated glass is used as the anode, which is separated from the cathode by a Teflon spacer (1.0 mm thick). The cavity for plasma generation is fabricated by cutting a circular hole (~10 mm in diameter) out of the Teflon spacer. The Ar plasma is triggered using a pulsed direct current voltage with bipolar pulse mode (20 μs square pulse, 6 kHz repetition rate) in Ar atmosphere under a pressure of 100 torr.

3. Results and Discussion

Figure 1 shows the processes for preparing patterns of Si nanostructure and transferring graphene on SiTs. The mask containing patterned arrays is fabricated using the conventional photolithographic process. A photoresist pattern is utilized to fabricate high quality Si nanostructures and to subsequently form SiT arrays. Figure 2a shows an FESEM image of typical SiT arrays. The inset of Figure 2a shows the magnified FESEM image of a single SiT, indicating that the SiT tips, which are 1.0 μm tall and sharp are successfully prepared on the Si substrate. High quality monolayer graphene is synthesized on Cu using the chemical vapor deposition method[32]. The variation in thickness and the graphitic quality of the graphene films are further evaluated by Raman spectroscopy. The Raman spectrum of the graphene film on Cu (graphene/Cu) foil [curve I of Figure 2b] shows the prominent peak of the D band at 1350 cm^{-1} which is associated with disordered sp^3-hybridized carbon featured as defects or impurities in carbon materials; the G band at 1580 cm^{-1} resulting from the E_{2g} vibration mode of sp^2 bonded carbon is also observed; the symmetric and sharp 2D band at 2689 cm^{-1} referring to the second-order vibration caused by the scattering of phonons at the zone boundary too is clearly visible[33]. It has been reported that there is a correlation between the ratio of I_{2D}/I_G and the number of layers in a graphene film. That is, I_{2D}/I_G decreases with the increase of layer numbers and a value greater than 2.0 indicates the presence of monolayer graphene[32]. The I_{2D}/I_G value is 2.07 for graphene/Cu foil, confirming the synthesis of monolayer graphene on Cu foil in this work.

The FESEM image shown in Figure 2c shows that the SiT arrays are fully covered by the monolayer graphene. The inset of Figure 2c clearly illustrates that the graphene monolayer forms a transparent layer and that the surface of the SiT arrays is clearly visible through the graphene layer. Moreover, the monolayer graphene forms nanometer-scale sharp protrusions (when it is used on the surface of the SiT arrays), which is observed from the magnified FESEM image in Figure 2d. The graphene on SiT arrays [curve II of Figure 2b] shows characteristic peaks of the Raman spectrum similar to those observed in the spectrum for the graphene/Cu foil [curve I of Figure 2b], indicating that the monolayer graphene maintains its high quality structure even after been transferred to the SiT arrays.

The thickness of the as-grown graphene transferred from the Cu foil onto SiT arrays is estimated from the atomic force microscopy (AFM) measurements. The height of the graphene monolayer with respect to Si substrate is measured to be about 0.4~0.7 nm (Figure 3a), consistent with the previous AFM observation of monolayer graphene[34], and this is thicker than the ideal thickness of 0.34 nm. High resolution (HR) TEM of the graphene is used to assess its quality and to determine the number of layers. Figure 3b shows the HRTEM image of a graphene/Si tip in our sample and the associated Fourier transformed diffractogram image (inset of Figure 3b).

The SiT arrays covered with graphene possess the same sharpness as the as-prepared SiT arrays, the separation between the tips being large enough to alleviate the electric field screening effect. As a result, the field emission property of the devices can be significantly improved. Figure 3a shows the J_e–E characteristics of the bare SiTs, graphene/Cu foil and graphene/SiTs. We observe no

Cite this: DOI: 10.1039/c0xx00000x

www.rsc.org/xxxxxx

ARTICLE TYPE

measurable field emission from the reference Si substrate even up to the maximum applied electric field of 70 V/μm; in addition, we also observed negligible field emission from the bare SiT arrays with a turn-on field of 23.40 V/μm and relatively low EFE current density of 0.078 mA/cm^2 at an applied field of 18.5 V/μm [curve I, Figure 4a]. In contrast, graphene/SiTs demonstrated extremely high emission current density of 3.04 mA/cm^2 at an applied field of 9.07 V/μm [curve III, Figure 4a]. The turn-on field (6.0 V/μm) of the graphene/SiTs is much lower than that of bare SiTs and lower than that of the well-aligned graphene arrays field emitters reported in Huang`s work[5]. For comparison we have also measured the EFE property of graphene/Cu foil [curve II, Figure 4a] and found that its EFE characteristics are not as efficient as that of the graphene/SiT arrays.

The EFE data is analyzed using the Fowler–Nordheim (F-N) equation[35], which describes the tunneling of field-assisted electrons from cathode to anode in vacuum under a high applied field. This relation has been widely used to describe the relationship between the current density J_e and the local field E_{loc} of the emitter using the equation $E_{loc}= \beta E$, where β is the field enhancement factor. In this regard, the F-N equation can be written as:

$$J_e = (A\beta^2E^2/\varphi) \exp(-B\varphi^{3/2}/\beta E)$$

where $A = 1.54 \times 10^{-6}$ A eV V^{-2} and $B = 6.83 \times 10^9$ eV$^{-3/2}$ V m^{-1}, E is the applied field and φ is the work function of the emitting materials. The plot of ln (J_e/E^2) versus 1/E yields a line in good agreement with the F–N equation. The intrinsic straight line of the F–N plot indicates that the current is due to electron field emission. The inset of Figure 4a shows F-N plots of the acquired data. The corresponding field enhancement factors are determined by fitting the linear part of the data according to the F-N equation. By assuming the work function of graphene to be 5 eV, the β values of graphene/SiTs and bare SiTs, calculated based on the slopes of F-N plots tested under high electric field, are approximately 1000 and 205, respectively. The significant increase in field enhancement factor β is greatly attributed to the geometrical factors such as high density of emitters, small curvature radius,[36] and the relatively large diameter of Si nanowire or nanotip is considered to be a limitation to further improve the FE property of Si nanostructures.[37] It is well-known that graphene has the high electrical conductivity and good field emission properties due to geometrical field-enhancement effect form the its protruding edge effect of the sheet boundary peripheral region. The presence of edges plays a key role for the electron transport and enabling to easier emitting of electrons into vacuum for graphene/ SiT. The field emission results of graphene/Cu were not better than graphene/Si tips due to the deposition methods, which lead to the graphene have the planar morphology along the entire substrates and it limits the field enhancement (curve II, Figure 4a). When the monolayer graphene was transferred on Si tips, the EFE properties predominated by the graphene rather than Si tips. The conductivity of Si tips is lower in comparison with graphene, while enhanced EFE measurements were due to large amounts electron emissions from sharp protrusions of graphene.

Stability of the field emission current is an important parameter related to potential applications. Disregarding short-term fluctuations due to adsorption and desorption of residual gas molecules and diffusion of adsorbed species on the emitter surface, we present a curve correlating J_e and operation time of the graphene/SiT arrays [curve II, Figure 4b] for a study performed over a period of 200 min at an applied voltage of 800 V. As seen from the figure, the insignificant variation in emission current indicates no obvious discharges or spikes over time, indicating a more stable performance of the graphene/SiT arrays in comparison with that of the bare SiT arrays [curve I, Figure 4b]. Uniform electron emission from the graphene/SiT arrays can be confirmed from the luminescence of the phosphor-coated anode at a voltage of 800 V, as shown in the inset of Figure 4b. The high stability of graphene/SiT arrays due to the homogeneity of graphene films,[6] whereas the less stability of SiT arrays is probably due to ion bombardment of residual gas molecules and joule heating can cause faster degradation of SiT martials.[38,39] The damaged sharp tips of SiT emitters are suffering from the excessive emission. Therefore graphene covered SiT arrays were executed the high emission currents with longer stability.

A more fascinating phenomenon is that the graphene/SiT arrays enhance markedly the PI properties of the plasma device while it is being utilized as a cathode. Figure 5a shows a series of photographs of the illumination behavior of these two plasma devices which utilize the bare SiTs [image series I, Figure 5a] and the graphene/SiTs [image series II, Figure 5a] as emitters. The intensity of the plasma increases monotonically with the applied voltage; the bare SiTs-based microplasma devices need 250 V to trigger the plasma [J_{pl}-V curve I, Figure 5 (b)] , while the graphene/SiTs-based microplasma devices can be triggered at a lower voltage of 220 V [J_{pl}-V curve I, Figure 5 (b)]. The PI characteristics are better illustrated by the variation of the plasma current density (J_{PI}) with respect to voltage, which is plotted in Figure 5b. The bare SiTs-based microplasma devices [curve I of Figure 5b] achieve a J_{PI} value of 1.85 mA/cm^2 at an applied voltage of 400 V, whereas the J_{PI} reaches the value of 2.0 mA/cm^2 at an applied voltage of 370 V for graphene/SiTs device [curve II of Figure 5b].

To evaluate the stability of the bare SiT and the graphene/SiT arrays, the plasma current is monitored over a long period with a constant applied voltage of 350 V. The plasma current of 0.33 mA is upheld for a period over 140 min, showing high life-time stability for graphene/SiTs-based microplasma devices [upper inset and curve II, Figure 5c]. In contrast, the plasma current of the bare SiT arrays [curve I, Figure 5c] decreases continuously during operation and the intensity of the PI for the microplasma devices is abruptly reduced at 20 min [bottom inset, Figure 5c]. This suggests that the better PI performance of the microplasma devices based on the graphene/SiTs, as compared with the bare SiTs-based ones, is closely associated with the better robustness of graphene/SiTs-based electron field emitters.

4. Conclusions

In conclusion, we demonstrate a simple and reproducible method of producing heterostructures of graphene/SiTs with excellent EFE and PI performances. The PI characteristics of the microplasma devices using these heterostructures are closely correlated to the EFE behaviour of the cathode materials. The graphene/SiT are fabricated by a transferring process, in which the well-aligned SiT arrays can be successfully covered by monolayer graphene. This work demonstrates that the transferring process leads to graphene/SiT field emitters producing high current density at low turn-on field. The PI current density value of $(J_{PI})_{graphene/SiTs} = 2.0$ mA/cm^2 (at an applied voltage of 370 V) is attained when the graphene/SiT emitters are used as the cathode. This material has the potential to make a considerable impact on graphene-based microplasma display technology.

Acknowledgements

The authors appreciate the financial support from the National Science Council through the project No. NSC 101-2221-E-007-064-MY3 and NSC 101-2112-M-032 -002.

Notes and references

*[a] *Department of Materials Science and Engineering, National Tsinghua University, Hsinchu, Taiwan 30013, Republic of China. Fax: +886 35737406; Tel: 88635715131 #42568; E-mail: nhtai@mx.nthu.edu.tw*
[b] Department of Engineering and System Science, National Tsinghua University, Hsinchu, Taiwan 30013, Republic of China.
**[c] Department of Physics, Tamkang University, Tamsui, Taiwan 25371, Republic of China.*
Fax: +886-2-26209917;Tel: +886-2-26268907; E-mail: inanlin@mail.tku.edu.tw

1 W. A. De Heer, A. Chatelain and D. Ugarte, *Science* 1995, **270**,1179.
2 S. Fan, M. G. Chapline, N. R. Franklin, T. W. Tombler, A. M. Cassell and H. Dai, *Science* 1999, **283**, 512.
3 J. Lee, Y. Jung, J. Song, J. S. Kim, G. W. Lee, H. J. Jeong and Y. Jeong, *Carbon* 2012, **50**, 3889.
4 Y. D. Lee, W. S. Cho, Y. C. Kim and B. K. Ju, *Carbon* 2012, **50**, 845.
5 C. K. Huang, Y. Ou, Y. Bie, Q. Zhao and D. Yu, *Appl. Phys. Lett.* 2011;**98**, 263104.
6 Z. S. Wu, S. Pei, W. Ren, D. Tang, L. Gao, B. Liu, F. Li, C. Liu and H. M. Cheng, *Adv. Mater.* 2009, **21**, 1756.
7 U. A. Palnitkar, R. V. Kashid, M. A. More, D. S. Joag, L. S. Panchakarla and C. N. R Rao, *Appl. Phys. Lett.* 2010, **97**, 063102.
8 H. Yamaguchi, K. Murakami, G. Eda, T. Fujita, P. Guan, W. Wang, C. Gong, J. Boisse, S. Miller, M. Acik, K. Cho, Yves J. Chabal, M. Chen, F. Wakaya, M. Takai and M. Chhowalla, *ACS Nano* 2011, **5**, 4945.
9 D. Ye, S. Moussa, J. D. Ferguson, A. A. Baski, M. S. El-Shall, *Nano Lett.* 2012, **12** ,1265.
10 S. Wang, J. Wang, P. Miraldo, M. Zhu, R. Outlaw, K. Hou, X. Zhao, Brian C. Holloway, D. Manos, T. Tyler, O. Shenderova, M. Ray, J. Dalton and G. McGuire. *Appl. Phys. Lett.* 2006, **89**, 183103.
11 M. Y. Zhu, R. A. Outlaw, M. Bagge-Hansena, H. J. Chen, D. M. Manos. *Carbon* 2011, **49**, 2526.
12 G. R. Gu and T. Ito, *Appl. Surf. Sci.* 2011, **257**, 2455,.
13 K. S. Novoselov, A. K. Geim, S. V. Morozov, D. Jiang, Y. Zhang, S. V. Dubonos, I. V. Grigorieva, A. A. Firsov, *Science* 2004, **306**, 666.
14 A. K. Geim and K. S. Novoselov, *Nat. Mater.* 2007, **6** ,183.
15 Y. Kopelevich and P. Esquinazi, *Adv. Mater.* 2007, **19**, 4559.
16 M. Qian, T. Feng, H. Ding, L. Lin, H. Li, Y. Chen and Z. Sun, *Nanotechnology* 2009, **20**, 425702.
17 A. Malesevic, R. Kemps, A. Vanhulsel, M. P. Chowdhury, A. Volodin and C. V. Haesendonck. *J. Appl. Phys.* 2008, **104**, 084301.
18 Y. Zhang, S. Tang, D. L. Deng, S. Z. Deng, J. Chen and N. S. Xu, *Carbon* 2013, **56**,103.
19 X . Wang, J. Zhou, C. Lao, J. Song, N, Xu and Z. L. Wang, *Adv. Mater.* 2007, **19**, 1627.
20 J. Liu, Z. Zhang, Y. Zhao, X. Su, S. Liu and E. Wang, *Small* 2005, **1**, 310.
21 H. Zeng, X. Xu, Y. Bando, U. K. Gautam, T. Zhai, X. Fang, B. Liu and D. Golberg. *Adv. Funct. Mater.* 2009, **19**, 3165.
22 Y. F. Tzeng, H. C. Wu, P. S. Sheng, N. H. Tai, H. T. Chiu, C. Y. Lee and I. N. Lin, *ACS Appl. Mater. Interface* 2010, **2**, 331.
23 X. S. Fang, Y. Bando, G. Z. Shen, C. H. Ye, U. K. Gautam, P. M. F. J. Costa, C. Zhi, C. C. Tang and D. Golberg, *Adv. Mater.* 2007, **19**, 2593.
24 Y. B. Guo, H. B. Liu, Y. J. Li, G. X. Li, Y. J. Zhao, Y. L. Song and Y. Li, *J. Phys. Chem. C* 2009, **113**, 12669.
25 U. K. Gautam, X. S. Fang, Y. Bando, J. H. Zhan and D. Golberg, *ACS Nano* 2008, **2**, 1015.
26 T. H. Chang, K. Panda, B. K. Panigrahi, S. C. Lou, C. L. Chen, H. C. Chan, I. N. Lin and N. H. Tai, *J. Phys. Chem. C* 2012, **116**, 19867.
27 T. H. Chang, S. C. Lou, H. C. Chen, C. L. Chen, C. Y. Lee, N. H. Tai and I. N. Lin, *Nanoscale* 2013, **5**, 7467.
28 U. N. Maiti, S. Maiti, T. P. Majumder and K. K. Chattopadhyay. *Nanotechnology* 2011, **22**, 505703.

Cite this: DOI: 10.1039/c0xx00000x

www.rsc.org/xxxxxx

ARTICLE TYPE

29 E. Stratakis, G. Eda, H. Yamaguchi, E. Kymakis, C. Fotakis and M. Chhowalla. *Nanoscale* 2012, **4**, 3069.
30 W. Kern, *J. Electrochem. Soc.* 1990, **137**, 1887.
31 Z. Huang, H. Fang and J. Zhu, *Adv. Mater.* 2007, **19**, 744.
32 X. S. Li, W. W. Cai, J. H. An, S. Kim, J. Nah, D. X. Yang, R. Piner, A. Velamakanni, I. H. Jung, E. Tutus, S. K. Banerjee, L. Colombo and R. S. Ruoff, *Science* 2009, **324**, 1312.
33 F. Tuinstra and J. Koenig, *J. Chem. Phys*. 1970, **53**, 1126.
34 K. S. Novoselov, A. K. Geim, S. V. Morozov, D. Jiang, Y. Zhang, S. V. Dubonos, I. V. Grigorieva and A. A. Firsov, *Science*, 2004, **306**, 666.
35 R. H. Fowler and L. Nordheim, *Proc. R. Soc.Lond. A*. 1928, **119**, 173.
36 C. X. Xu and X. W. Sun, *Appl. Phys. Lett.* 2003, **83**, 3806.
37 Y. F. Tzeng, H. C. Wu, P. S. Sheng, N. H. Tai, H. T. Chiu, C. Y. Lee and I. N. Lin, *ACS Appl. Mater. Interface* 2010, **2**, 331.
38 C. Y. Hong and A. I. Akinwande, *IEEE Trans. Electron Devices* 2005, **52**, 2323.
39 J. M. Bonard and C. Kinke, *Phys. Rev. B* 2003, **67**, 115406.

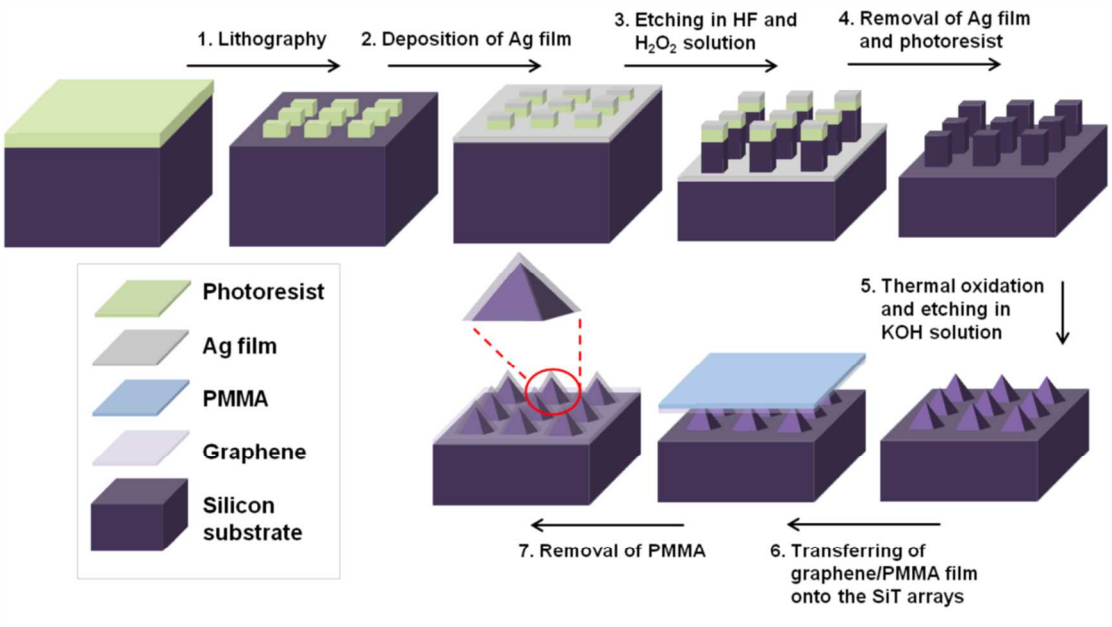

Figure 1. The schematics of the processes for transferring graphene onto the Si tip array templates: (1) patterning of photoresist by an optical lithographic process, (2) deposition of Ag-interlayer, (3) acid etching for forming Si-rods, (4) removal of photoresist and Ag-interlayer, (5) thermal oxidation and etching in KOH solution to sharpen the Si tips, (6) PMMA/graphene film transferred onto the Si tips, and (7) removal of PMMA by acetone to obtain the sample with graphene uniformly covered on the Si tips.

Cite this: DOI: 10.1039/c0xx00000x

www.rsc.org/xxxxxx

ARTICLE TYPE

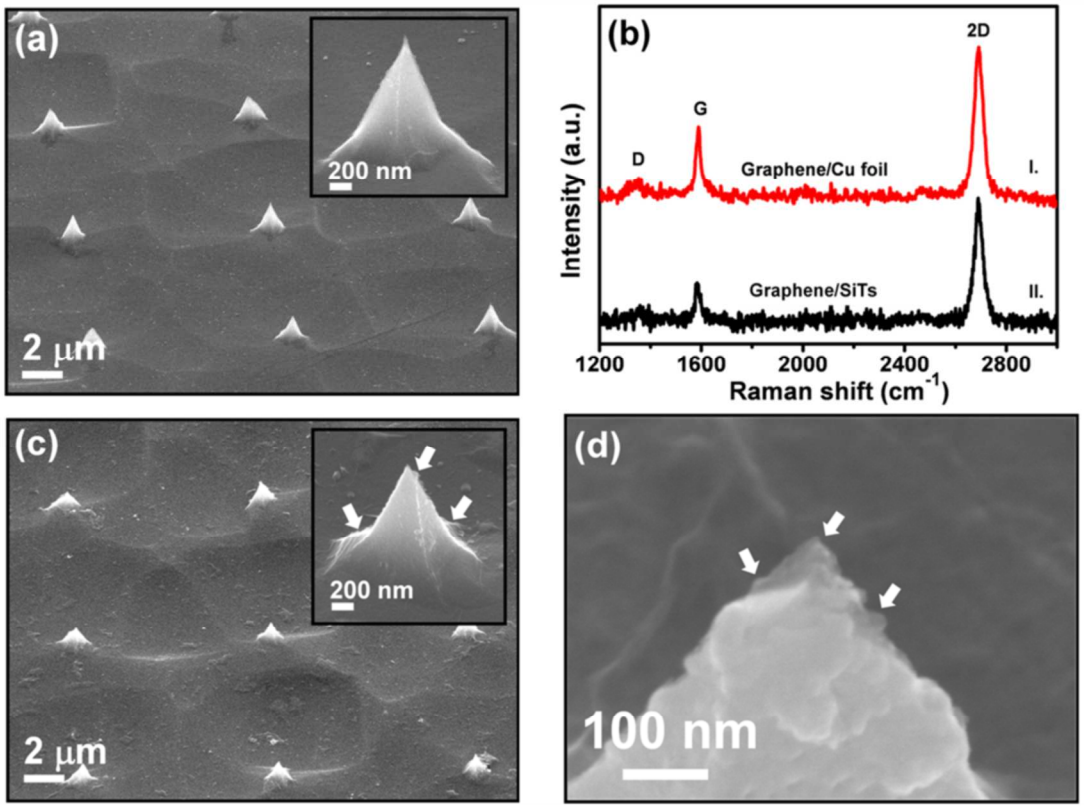

Figure 2. (a) The SEM images of the Si tip without protruding graphene, in which the inset of (a) shows the single Si tip; (b) Raman spectra of monolayer graphene on the reference graphene/Cu foil (curve I) and graphene/SiT arrays (curve II); (c) The surface of the SiT arrays covered with graphene, and the inset depicting the Si which can be clearly observed through the graphene; (d) Monolayer graphene with protrusion on SiTs.

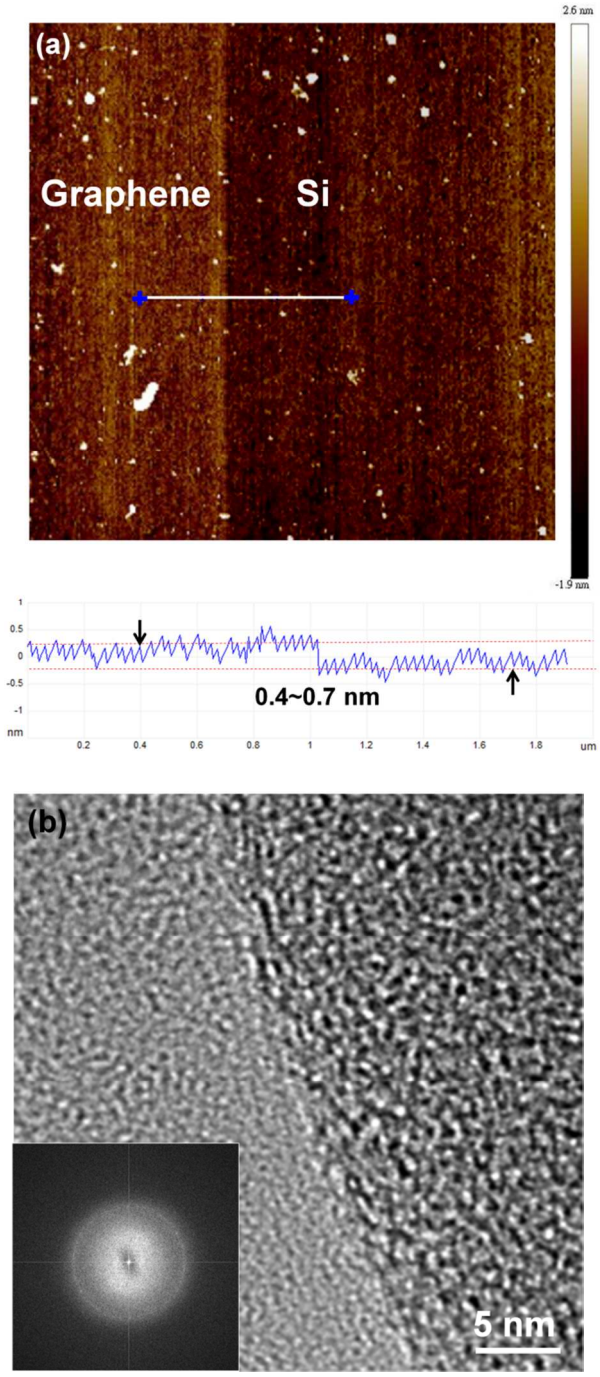

Figure 3. (a) Depicts the AFM image of the graphene/Si tip. The height of the monolayer graphene layer over the Si tip is about 0.4-0.7 nm. (b) Shows the corresponding HRTEM image of the graphene/Si tip, and the inset showing the Fourier transformed diffractogram image image corresponding to the whole image.

Cite this: DOI: 10.1039/c0xx00000x

www.rsc.org/xxxxxx

ARTICLE TYPE

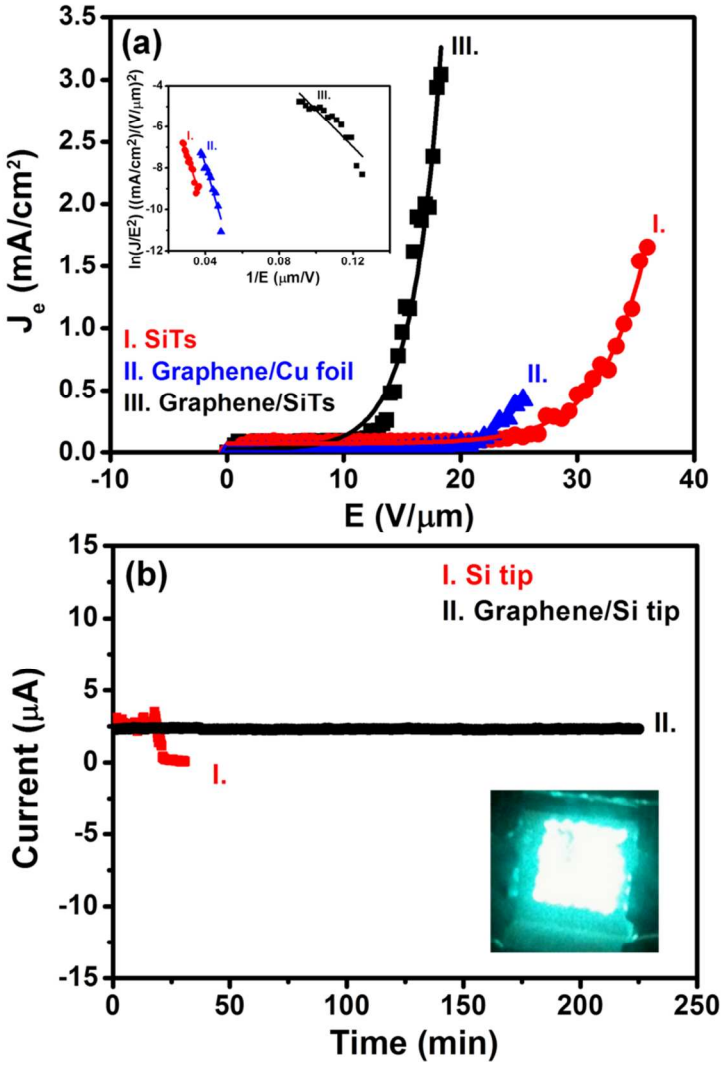

Figure 4. (a) Field emission current density (J_e) versus applied electric field (E) of bare SiTs, graphene/Cu foil and the graphene/SiT emitters (the inset shows the Fowler-Nordheim plots, i.e., $\log(J_e/E^2)$-$1/E$ plots); (b) stability measurement, i.e., current versus time of (I) bare SiTs and (II) graphene/SiT emitters with the inset showing the luminous field emission device using graphene/SiTs as cathode.

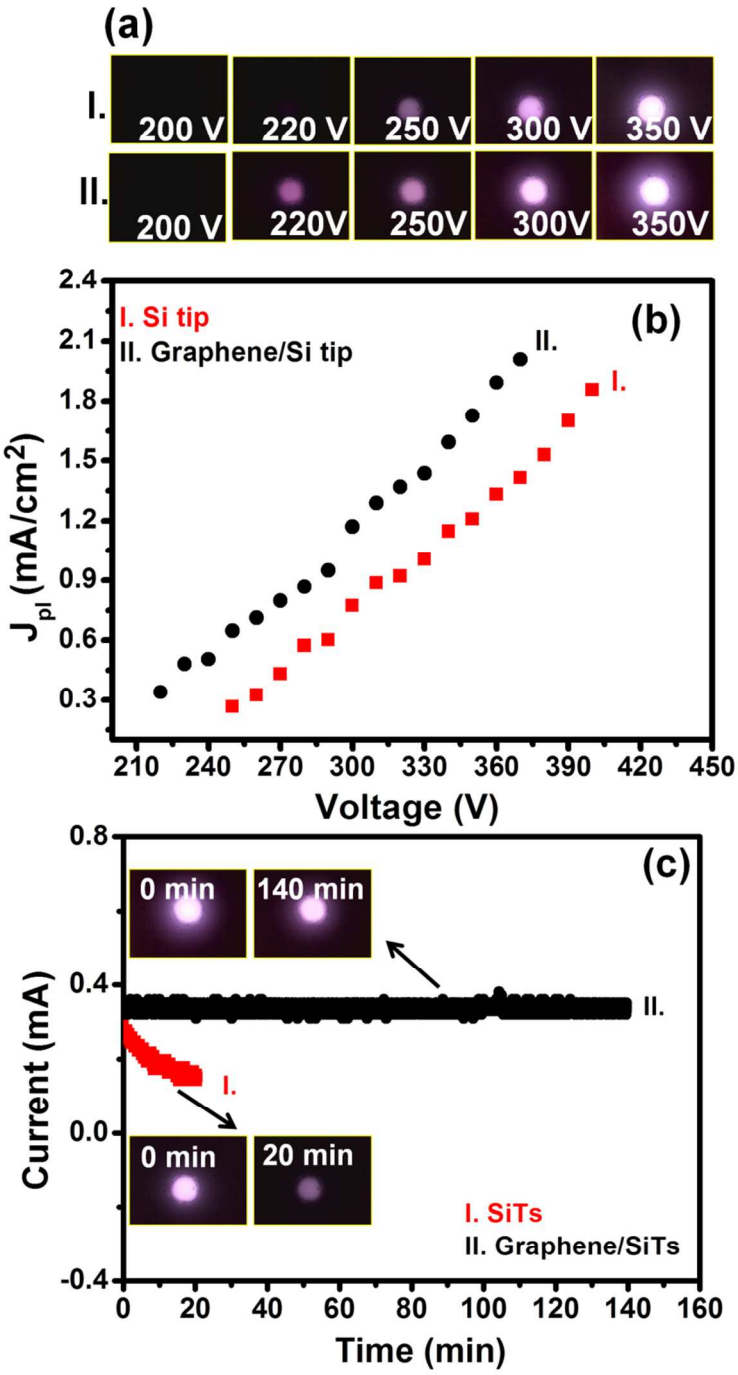

Figure 5. (a) The PI behavior showing the plasma images versus the applied voltage of the microplasma devices, (b) the plasma current density versus applied field of the microplasma devices and (c) the plasma current stability using (I) bare SiTs and (II) graphene/SiTs as cathode. The upper inset in (c) shows the PI stability of graphene/SiT arrays at durations of 0 min and 140 min, whereas the bottom inset shows the PI stability of bare SiT arrays at durations of 0 min and 20 min at an applied voltage of 350 V.

Cite this: DOI: 10.1039/c0xx00000x

www.rsc.org/xxxxxx

ARTICLE TYPE

Table of Contents

High efficiency with excellently stable electron field emitters based on monolayer graphene coated on well-aligned Si tip (graphene/SiT) arrays fabricated by a simple transfer method is demonstrated. The novel heterostructure of the monolayer graphene supported on vertical SiTs provides the protruded nanostructure, which locally enhances the electric field and thus improves the field emission and the plasma illumination characteristics.

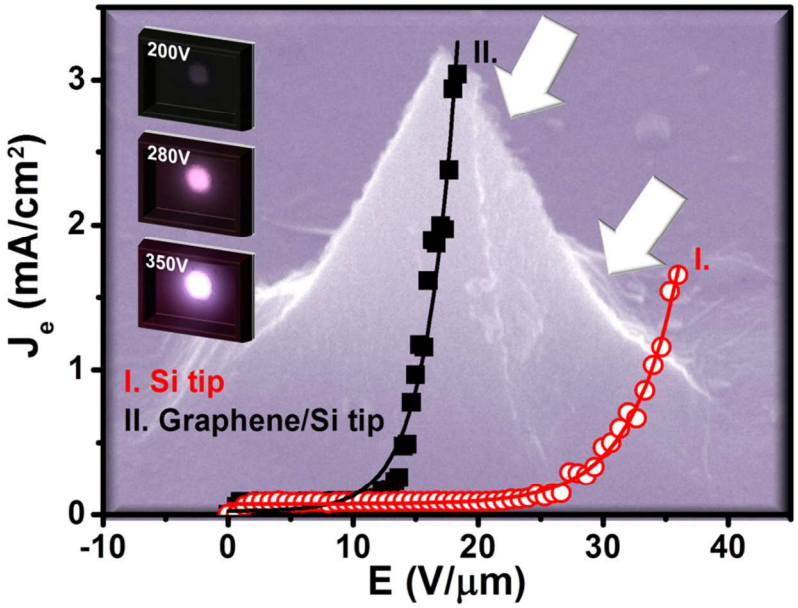

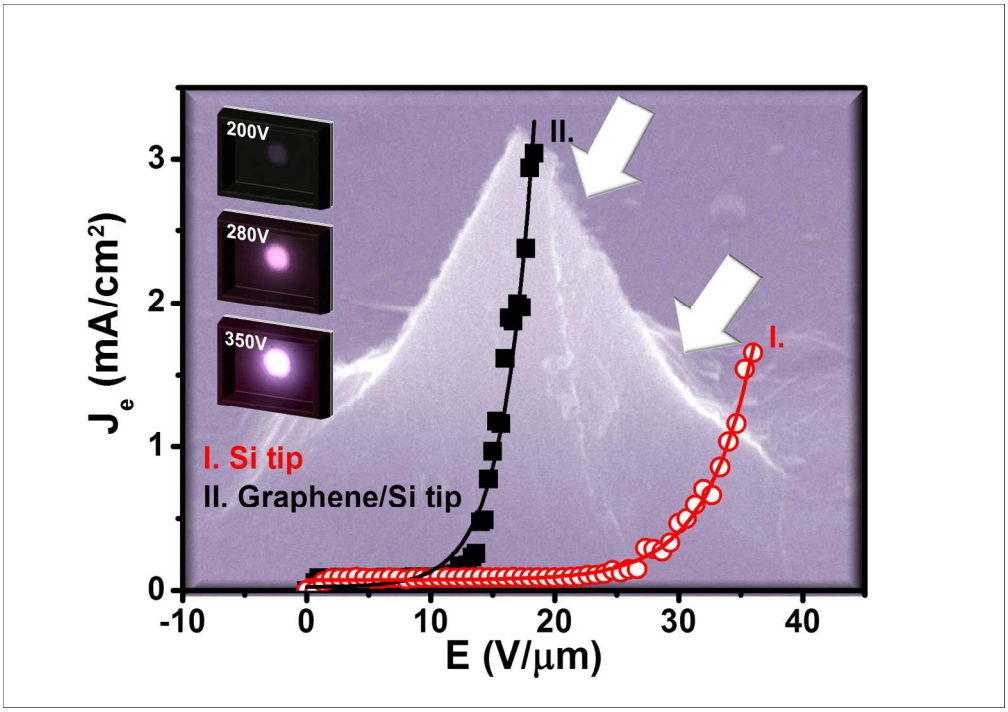

High efficiency with excellently stable electron field emitters based on monolayer graphene coated on well-aligned Si tip (graphene/SiT) arrays fabricated by a simple transfer method was demonstrated. The novel heterostructure of the monolayer graphene supported on vertical SiTs provided protruded nanostructure, which locally enhanced the electric field and thus improved the field emission and the plasma illumination characteristics.
422x296mm (150 x 150 DPI)